

Deep Crisp Boundaries: From Boundaries to Higher-level Tasks

Yupei Wang, *Student Member, IEEE*, Xin Zhao, *Member, IEEE*, Yin Li, *Member, IEEE*,
and Kaiqi Huang, *Senior Member, IEEE*

Abstract—Edge detection has made significant progress with the help of deep Convolutional Networks (ConvNet). ConvNet based edge detectors approached human level performance on standard benchmarks. We provide a systematical study of these detector outputs, and show that they failed to accurately localize edges, which can be adversarial for tasks that require crisp edge inputs. In addition, we propose a novel refinement architecture to address the challenging problem of learning a crisp edge detector using ConvNet. Our method leverages a top-down backward refinement pathway, and progressively increases the resolution of feature maps to generate crisp edges. Our results achieve promising performance on BSDS500, surpassing human accuracy when using standard criteria, and largely outperforming state-of-the-art methods when using more strict criteria. We further demonstrate the benefit of crisp edge maps for estimating optical flow, generating object proposals and semantic segmentation. In addition, the proposed refinement architecture can be easily generalized to saliency detection task, achieving state-of-art results on five commonly used saliency detection benchmark.

Index Terms—Boundary Detection, Crisp Boundaries.

I. INTRODUCTION

EDGE detection is a well-established problem in computer vision. Finding perceptually salient edges in natural images is important for mid-level vision [2]. Moreover, edge detection outputs, in terms of boundary maps, are often used for other vision tasks, including optical flow [3], object proposals [4] and object recognition [5]. We have witnessed a significant progress on edge detection, ever since our community embraced a learning based approach [6]. In particular, state-of-the-art methods [7], [8] such as Holistic Edge Detector [7] (HED), leveraging deep ConvNet for detecting edges, achieved human level performance on standard datasets such as BSDS500 [9].

Is edge detection a solved problem? In Figure 1(a), we show a visualization of human labeled edges, in comparison to outputs from HED (the current state-of-the-art) and PMI

Y. Wang and X. Zhao are with the Center for Research on Intelligent Perception and Computing, National Laboratory of Pattern Recognition, Institute of Automation, Chinese Academy of Sciences, Beijing 100190, China, and also with the University of Chinese Academy of Sciences, Beijing 100049, China. E-mail: wangyupei2014@ia.ac.cn, xzhao@nlpr.ia.ac.cn.

Y. Li is with School of Interactive Computing, College of Computing, Georgia Institute of Technology, 218 TSRB, Georgia Tech. E-mail: yli440@gatech.edu.

K. Huang are with the Center for Research on Intelligent Perception and Computing and National Laboratory of Pattern Recognition of Institute of Automation, Chinese Academy of Sciences, Beijing 100190, China, and also with the University of Chinese Academy of Sciences, Beijing 100049, China and are also with the CAS Center for Excellence in Brain Science and Intelligence Technology, 100190 (kquang@nlpr.ia.ac.cn).

A preliminary version of this work appeared in [1]

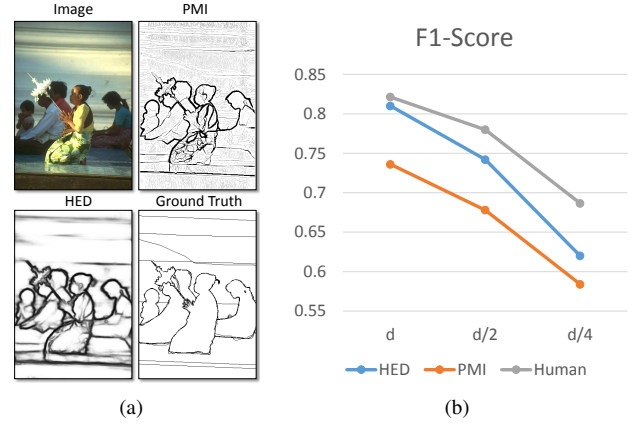


Fig. 1. (a) Visualization of edge maps from PMI [10] and HED [7] with input images and ground-truth edges; (b) Performance (on the left image) drops with decreased matching distance. With a tighter distance, the gap between PMI and HED decreases and the gap between HED and human increases. These results suggest that edges from HED are not well aligned with image boundaries. We seek to improve the localization ability of ConvNet based edge detector in this paper.

(designed for accurately localizing edges). While the HED result has a higher score, the quality of the edge map is less satisfactory—edges are blurry and do not stick to actual image boundaries. An accurate edge detector has to balance between “correctness” of an edge (distinguishing between edge and non-edge pixels) and “crispness” of the boundary (precisely localizing edge pixels) [10]. We can capture the “crispness” by decreasing the maximal permissible distance when matching ground-truth edges during benchmark. When we tighten the evaluation criteria (the maximal permissible distance decreases from d to $d/4$), the F1 score gap between HED and human increases and the gap between HED and PMI decreases (see Figure 1(b)).

Both qualitative and quantitative results suggest that edge maps from a ConvNet are highly “correct” yet less “crisp”—edges are not well localized. This issue is deeply rooted in modern ConvNet architecture [11]. First, spatial resolution of features is drastically reduced in more discriminative top layers due to the successive pooling layers, leading to blurred output of edges. Second, because of the large receptive field, fully convolutional architecture encourages similar responses of neighboring pixels, and thus may fail to produce a thin edge map. Such a thick and blurred edge map can be adversarial for other vision tasks [10]. For example, recent optical flow methods [12], [3] require accurate and crisp edge inputs to

interpolate sparse matching results, and thus may have sub-optimal performance with blurry edges.

We address this challenging problem of learning a crisp edge detector using ConvNet, and seek to improve the localization ability of HED. To this end, we propose a novel refinement architecture, inspired by the recent advance in dense image labeling [13], [14]. Our method equips an crisp edge detection (CED) network with a top-down backward-refining pathway, which progressively increases the resolution of feature maps using efficient sub-pixel convolution [14]. The refinement pathway adds additional non-linearity to the network, further reducing the correlation between edge responses within neighboring pixels. Our method achieves promising results on BSDS500, surpassing human performance when using standard criteria, and largely outperforming state-of-the-art methods when using more strict evaluation criteria. What's more, since backbone network is critical for deep learning approaches, we improve HED and our CED with state-of-the-art backbone network [15] and additional convolutional layers at all side-outputs[16]. Improved CED achieves new state-of-the-art performance on BSDS500. And we also give insight into the crispness of the original CED and improved CED.

Boundary detection serves as the basis for other higher-level vision tasks. EpicFlow [3], a state-of-the-art optical flow estimation method, performs edge-preserving interpolation from sparse matches for accurate dense matching. Some object proposal generation methods also need accurate edge prediction localized well around object boundaries, such as MCG [4] which computes hierarchical segmentation with predicted object boundaries. As a post-processing step for standard FCN-based [17] semantic segmentation method, BNF [18] computes precise object boundaries to refine blob-like and poorly localized predictions generated by FCN. Through three comparative experiments (especially for a comparison between our method and original HED), we demonstrate the benefits of crisp edges for optical flow, object proposals and semantic segmentation.

Finally, we demonstrate the proposed network can be easily extended to other related tasks, such as saliency detection [19]. Both ConvNet-based boundary detection and salient region detection method output a response map with the same resolution as original image. And each pixel in the response map indicates the probability of corresponding pixel in the input image to be boundary of a object or belong to a salient region. So the CED network for boundary detection can be easily adapted to salient region detection. In this way, we achieves state-of-the-art results on five commonly used salient detection datasets, indicating the generality of CED network.

Our contributions are thus summarized into four parts.

- We provide a systematical study of edge maps from ConvNet. We show that ConvNet is good at classifying edge pixels yet has poor localization ability.
- We combine the refinement scheme [13] with sub-pixel convolution [6] into a novel architecture, which is specifically designed for learning crisp edge detector. Our results on BSDS500 outperform state-of-the-art methods on all matching distances.

- We show that crisp edge maps can improve optical flow estimation, object proposals generation and semantic segmentation.
- We demonstrate the generality of our proposed network via the saliency detection task. State-of-the-art results are achieved on five commonly used saliency detection datasets without architecture modifications.

We organize our paper as follows. Section II reviews related work on edge detection. Section III presents our study of edge maps from ConvNet. Section IV details our method. Section V demonstrates experimental results for boundary detection. Section VI shows the benefits of crisp boundaries. Finally, section VII illustrates generality of our proposed network to saliency detection.

II. RELATED WORK

There is a vast literature on the classical problem of edge detection. A complete survey is out of scope for this paper. We only review a subset of relevant works in this section.

Early edge detectors are manually designed to find discontinuities in intensity and color [20], [21], [22]. Martin et al. [2] found that adding texture gradients significantly improves the performance. Most recent works explore learning based approaches for edge detection. Dollár et al. [6] proposed a data-driven, supervised edge detector, where detection is posed as a dense binary labeling problem with features collected in local patches. Many modern edge detectors have followed this paradigm by using more sophisticated learning methods. For example, Lim et al. [23] proposed to cluster human generated contours into so called Sketch Tokens. They then learn a random forest that maps a local patch to these tokens, which is used to re-assemble local edges. This idea was further extended by Dollár and Zitnick. They proposed structured random forest that simultaneously learns the clustering and mapping, and directly outputs a local edge patch. Ren and Bao [24] combined features learned from sparse coding and Support Vector Machine (SVM) for edge detection. Their method can be considered as a two-layer neural network.

The recent success of deep ConvNet has greatly advanced the performance of edge detection. Bertasius et al. [25] computes multi-scale patch for candidate contour point generated by Canny detector [21], then two branches convolutional network are used to classify and regress the patch. Shen et al. [26] proposed to cluster contour patches with different shape and defined a positive-sharing loss shared among each shape class. Instead of depending on low-level cues, Bertasius et al. [27] tried to exploit high-level object-related features for boundary detection. They achieved this by presenting a deep network which consists of pretrained convolutional layers. Xie and Tu [7] proposed to combine fully convolutional networks [28] with deep supervision [29]. Their method leverages features from different scales using skip-layer connections and has achieved a superior performance (within 2% gap to human level). Kokkinos et al. [8] further extended HED by adding multi-instance learning, more training samples and a global grouping step. Their results had surpassed human performance on BSDS500, although with

significantly more training images. Yang et al. [30] developed a fully convolutional encoder-decoder network for high-level object contour detection. In addition, Maninis et al. [31] proposed to model the orientation of edges, they also evaluate the proposed method on high-level tasks, such as semantic contours, semantic segmentation and object detection. Some recent work explored weakly supervised or unsupervised edge detection. Khoreva et al. [32] proposed to obtain object-specific boundaries without object boundary annotations at training phase and showed that bounding box annotations alone is sufficient to detect object boundary. Li et al. [33] presented an unsupervised learning pipeline for edge detection. However, these results tend to emphasis on the “correctness” of edges by selecting an optimistic matching distance,¹ and overlook the “crispness” of edges. In fact, the performance drops dramatically when the evaluation criteria is tightened. In contrast, our method builds on HED and seeks to improve its localization ability.

Our method is motivated by Isola et al. [10]. They proposed an affinity measure based on point-wise mutual information using distributions of hand-crafted local features. Edges are then detected using this affinity with spectral clustering. We share the same goal of designing a crisp edge detector yet our method and setting are completely different. More precisely, we pursue a learning based approach using ConvNet for crisp edges. Finally, our method is inspired by Pinheiro et al. [13], where a refinement architecture is proposed for segmenting objects. Our method adopts the top-down pathway of [13] to label the sparse binary signals of edges. We also replace the bilinear interpolation (deconvolution) with sub-pixel convolution [14], which is critical for generating better-localized, sharp edge output. Handle different vision tasks with same architecture has been explored in [34], [35], we demonstrate that our proposed network can achieve state-of-the-art performance on saliency detection even without modifications on network architecture.

III. THICK BOUNDARIES FROM CONVNET

We start by looking into the output edge maps of HED [7], a recent successful edge detector using ConvNet. HED predicts edge confidence at different layers of the network, leading to a set of edge maps. These maps are down-sampled due to successive pooling operations in the network. Then, they are further up-sampled to fit the input resolution by bilinear interpolation and averaged to produce the final edge map. We show an example of the edge map in Figure 2(a). Although the detector achieved a ODS of 0.78 on BSDS, the visual quality of the edge map is not satisfying. Edges look blurred and visually defective.

Why would such a blurry edge map reach a high score in benchmark? The standard evaluation [9] iterates over all confidence thresholds and uses bipartite graph matching to match between a binarized edge map to ground-truth edges. The matching is controlled by a maximal permissible distance d . A misaligned edge pixel is still considered correct as long as its distance to the nearest ground-truth is smaller than d

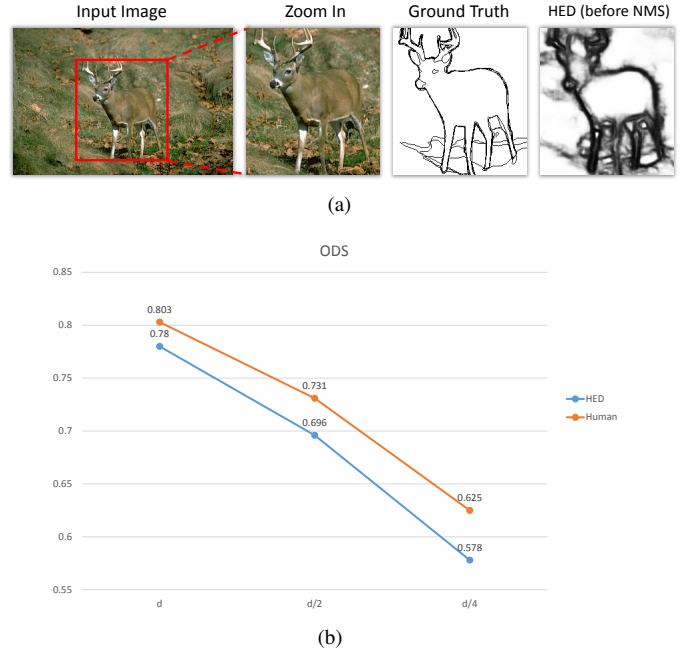


Fig. 2. (a) Thick and noisy edge map generated with HED [7] before non-maximal suppression (NMS); (b) Optimal Dataset Score (ODS) for both HED and human drop with decreased matching distance on the BSDS500 test set. However, the performance gap between HED and human increases from 2.3% to 4.7% as the distance decreases from d to $d/4$.

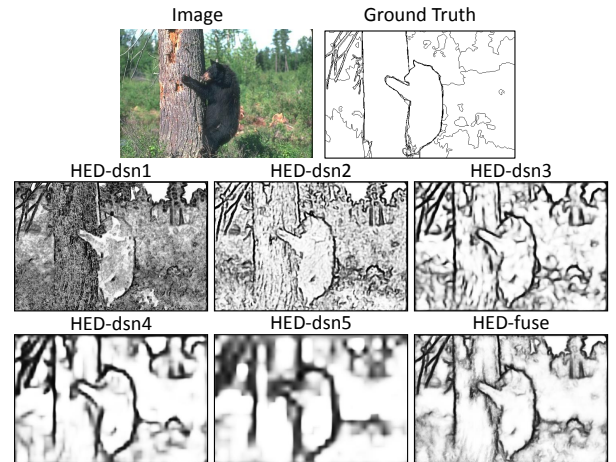


Fig. 3. Predictions from all side-output layers and final output of HED [7] (HED-fuse). The lower layers (HED-dsn1, HED-dsn2, HED-dsn3) capture more spatial details, while lack sufficient semantic information. On the contrary, the deeper layers (HED-dsn4, HED-dsn5) encode richer semantic information, but spatial details are missing.

pixels. With a optimistic d , we can achieve a good score even if edges are slightly shifted.

In fact, edge detection has to balance between “correctness” of an edge (distinguishing between edge and non-edge pixels) and “crispness” of the boundary (precisely localizing edge pixels) [10]. Crisp edges may be critical for other vision tasks, such as optical flow or image segmentation. “Crispness” can be measured by decreasing d in the benchmark. Human performance gradually decreases with smaller d , as we show in

¹4.3 pixels in a resolution of 321×481

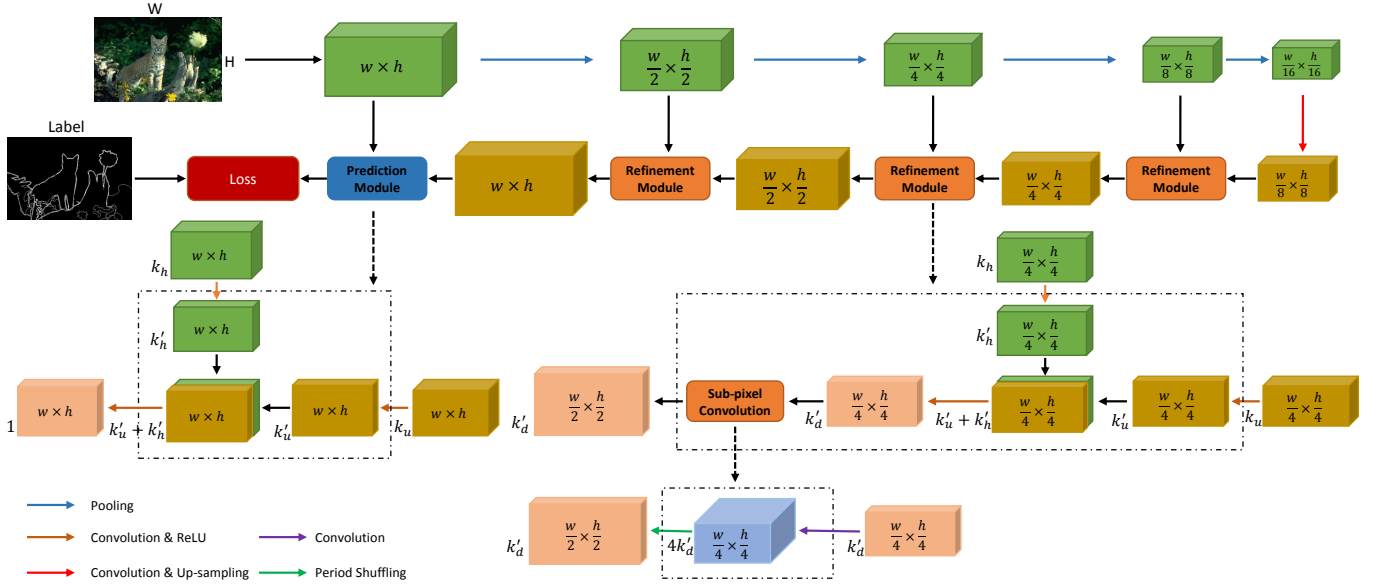


Fig. 4. Our method of Crisp Edge Detector (CED). We add a backward-refining pathway, which progressively increase the resolution of feature maps. Our refinement module fuses a top-down feature map with feature maps on the forward pass, and up-samples the map using sub-pixel convolution. This architecture is specially designed for generating edge maps that are well-aligned to image boundaries.

Figure 2(b). However, HED outputs show a more drastic drop, indicating that HED edges are not well aligned to actual image boundaries. This is in accordance with our visual inspection of the edge map.

IV. MAKE CONVOLUTIONAL BOUNDARIES CRISP

How can we make a crisp edge map from ConvNet? We start by analyzing the architecture of HED. Like modern ConvNets, spatial resolution of more discriminative top layers is significantly reduced due to the successive pooling operations. HED further attaches a linear classifier on layers with different resolution, and uses bilinear interpolation (realized as deconvolution) to up-sample their outputs to the original resolution. This design has two major issues. First, linear classifiers within the fully convolution architecture produce similar responses at neighboring pixels. It is thus difficult to distinguish an edge pixel from its neighbors. More importantly, simple up-sampling cannot recover original spatial details, and further blurs the edge map.

Architecture modifications are thus required for generating a crisp edge map. In this section, we address the challenging problem of designing a Crisp Edge Detector (CED) by proposing a novel architecture. Our method supplements HED network with a backward-refining pathway, which progressively up-samples features using efficient sub-pixel convolution [14]. CED is able to generate an edge map that is better aligned with image boundaries. We present details of CED and explain our design choices.

A. Architecture Overview

Figure 4 shows an overview of CED with two major components: the forward-propagating pathway and backward-refining pathway. The forward-propagating pathway is similar

to HED. It generates a high-dimensional low-resolution feature map with rich semantic information. The backward-refining pathway fuses the feature map with intermediate features along the forward-propagating pathway. This refinement is done multiple times by a refinement module. Each time we increase the feature resolution by a small factor (2x) using sub-pixel convolution, eventually reaching the input resolution. Details of our network are elaborated in following subsections.

B. Refinement Module

The skip-layer connection provides HED the important ability to use features at different layers for finding edges [7]. Figure 3 shows example edge map predictions from all side-output layers and final output edge map (HED-fuse). The lower layers (HED-dsn1, HED-dsn2, HED-dsn3) capture more spatial details, while lack sufficient semantic information. On the contrary, the deeper layers (HED-dsn4, HED-dsn5) encode richer semantic information, but spatial details are missing. HED simply averages independent predictions from all side-output layers. We argue that this is not a good design as it does not explore the hierarchical feature representations of ConvNet. To get a better fusion of the multi-layer features, we introduce the backward-refining pathway with refinement modules, similar to [13]. Note that our task of detecting sparse edges is significantly different from segmenting objects in [13]. Thus, directly applying the same module in [13] leads to sub-optimal performance.

The refinement module is repeated several times to progressively increase the resolution of feature maps. The key idea is to aggregate evidences of edges across the path using intermediate feature maps. Detailed structure of the module is shown in the bottom part of 4. Each module fuses a top-down feature map from the backward pathway with the feature map

from current layer in the forward pathway, and further up-samples the map by a small factor (2x), which is then passed down the pathway. There are two core components in this module, namely **fusion** and **up-sampling**.

Fusion: A straightforward strategy of fusion is to directly concatenate two feature maps. However, this is problematic since they have different number of feature channels. Directly concatenating the features risks drowning out the lower dimensional signal. Similar to [13], we match the number of feature channels between the two maps through dimension reduction. This is done by reducing the dimension of both feature maps through additional convolutional layers. We then concatenate the two low-dimensional feature maps with equal channels.

We denote the number of channels of the input forward pathway feature map as k_h . After the convolutional and ReLU operations, the channels are reduced to k'_h , which is much less than k_h . The same operations are conducted to the feature map from the previous refinement module to produce k'_u from k_u . We concatenate the above feature maps into a new feature map with $k'_u + k'_h$ channels and reduce it to a feature map with k'_d channels by a 3×3 convolutional layer as well. Thus, the overall computational cost is reduced and the two input feature maps are balanced.

Up-sampling: After fusion, our refinement module will also expand the resolution of feature maps. We up-sample the fused feature map with a sub-pixel convolution [36]. The sub-pixel convolution, different from the popular deconvolution for up-sampling [37], [38], [39], is a standard convolution followed by additional rearrangement of feature values, termed phase shift. It helps to remove the block artifact in image super-resolution task and maintain a low computational cost. We found that using sub-pixel convolution is important for better localization of edges.

Supposed we have i input channels and o desired output channels, the kernel size of a convolutional layer is denoted as (o, i, r, c) , where r and c stand for the kernel width and kernel height respectively. Considering output feature map with k times larger resolution than the input one, the traditional deconvolutional layer would employ the kernel size to be $(o, i, k \times r, k \times c)$. Instead of directly output enlarged feature map through a single deconvolutional layer, the sub-pixel convolution consists of one convolutional layer and one following phase shift layer. The kernel size of the convolutional layer is $(o \times k^2, i, r, c)$, thus generating feature map with $o \times k^2$ feature channels with identical resolution. Then we apply the phase shift to assemble the output feature map to the feature map with o feature channels but k times larger resolution in a fixed order.

Relationship to [7] and [13]: CED subsumes HED [7] as a special case, where 3×3 convolutions and ReLUs are replaced by linear classifiers and progressive up-sampling is used. Our method is different from [13] as we replace bilinear interpolation with sub-pixel convolution. This enables a more expressive model with a small number of extra parameters. Our task of edge detection is also different from object segmentation in [13].

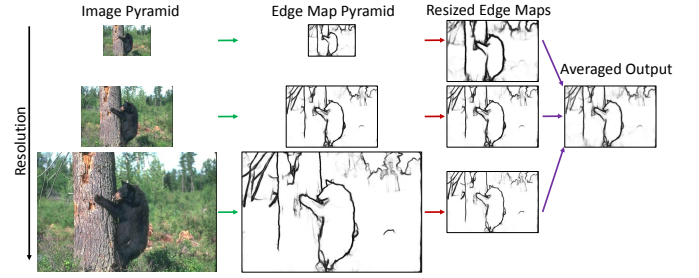


Fig. 5. Multi-scale fusion strategy for the evaluation stage.

C. Implementation Details

Our implementation builds on the publicly available code of HED [7], using Caffe as backend [40]. For training, we initialize the forward-propagating pathway with the pre-trained HED model. The other layers are initialized with Gaussian random distribution with fixed mean (0.0) and variance(0.01). The hyper parameters, including the initial learning rate, weight decay and momentum, are set to $1e - 5$, $2e - 4$ and 0.99, respectively.

For backward-refining pathway, the number of convolutional kernels is set to 256 for the top layer. This number is decreased by half along the path. For example, the first, second, and third top-down refinement module will have 128, 64 and 32 feature channels, respectively. Since the resolution of feature maps decreases by a factor of 2 after every pooling operation, the sub-pixel convolution up-samples the input feature map by 2x in each refinement module.

V. CRISP EDGE DETECTION

We conduct extensive experiments to benchmark CED. We first present our datasets and evaluation criteria. Our experiments start with an ablation study of network architecture. We further compare our best performing method with state-of-the-art methods on edge detection.

A. Datasets and Benchmarks

We evaluate edge detectors on the widely-used Berkeley Segmentation Dataset and Benchmark (BSDS500) dataset [2], [9]. It consists of 200 images for training, 100 for validation, and 200 for testing. Each image is annotated by multiple annotators. We use the train and validation set for training (similar to [7]) and report results on the test set. The performance is measured by the precision/recall curve that captures the trade-off between accuracy and noise [2]. In addition, three standard metrics are reported: fixed contour threshold (ODS), per-image best threshold (OIS) and average precision (AP).

B. Ablation Study

Our first experiment is to test different network architectures of CED. We use the original HED [7] network as our baseline. We trained different versions of CED with or without sub-pixel convolution (CED-w/o-Subpixel by using deconvolution

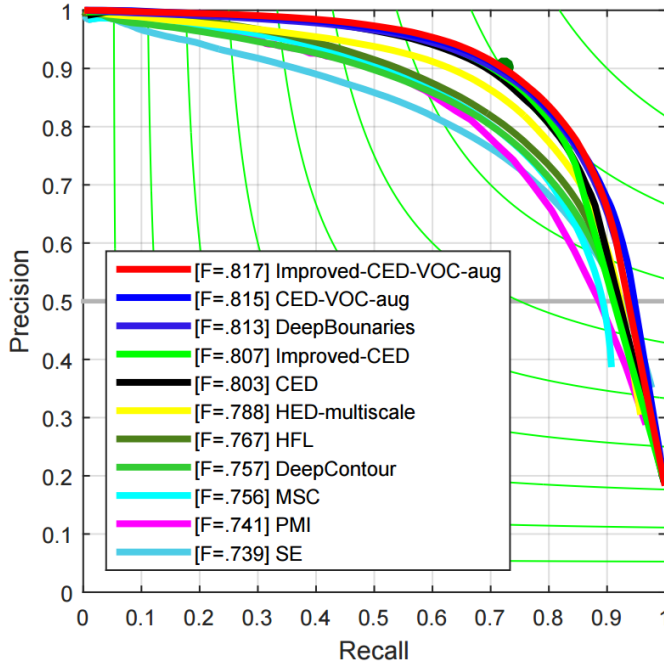


Fig. 6. Precision/Recall curves of different methods on BSDS500 dataset using standard evaluation criteria. CED is close to the best record by DeepBoundaries, which uses extra training data and post-processing steps. Simply augmenting training data as DeepBoundaries, without any post-processing, CED-VOC-aug achieves state-of-the-art result. As CED-VOC-aug, without complex post-processing steps, Improved-CED-VOC-aug surpasses all previous state-of-arts.

instead). This is carried out to prove the effectiveness of sub-pixel convolution. It is worth noting that both CED and CED-w/o-Subpixel are initialized by the same model. Moreover, we tested the multi-scale fusion strategy for the evaluation. In this case, a testing image is resized to three different resolutions ($1/2x$, $1x$, $2x$), which are fed into the same network independently. Finally, we resize the three output edge maps to the original resolution, and average them to generate the final edge map. Fig.5 shows the pipeline of the multi-scale fusion strategy for the evaluation.

In training, we adopt a modified version of consensus sampling strategy [7] to prevent the problematic convergence behavior. A pixel is assigned positive label if it is labeled as edge by at least three annotators. Pixels have not been labeled by any annotators are treated as negative. The rest of the pixels are ignored during training (by blocking their gradients). We also augment the data by rotating, cropping and multi-scale resizing. Our results are summarized in Table I. Our refinement module improves over the baseline HED by 1%, sub-pixel convolution further boosts the performance by 1.4% and multi-scale testing adds another 0.9%. Our full model improves the ODS from 0.780 to 0.803, slightly higher than human performance of 0.8027. These results demonstrate the effectiveness of CED.

C. Boundary Detection

We further compare the best performing version of CED to state-of-the-art methods in Table II. Fig. 6 shows Precision-

Method	ODS	OIS	AP
HED	.780	.797	.829
CED-w/o-Subpixel-w/o-Multi	.793	.811	.838
CED-w/o-Multi	.794	.811	.847
CED-w/o-Subpixel	.800	.819	.859
CED	.803	.820	.871

TABLE I
RESULTS ON BSDS500 WITH DIFFERENT NETWORK ARCHITECTURE SETTINGS. CED-W/O-MULTI REFERS TO CED WITHOUT MULTI-SCALE TESTING, SIMILAR FOR CED-W/O-SUBPIXEL-W/O-MULTI.

Method	ODS	OIS	AP
Human	.8027	.8027	-
gPb-owt-ucm[9]	.726	.757	.696
SE-Var[41]	.746	.767	.803
PMI[10]	.741	.769	.799
MES[42]	.756	.776	.756
DeepEdge [43]	.753	.769	.784
MSC [44]	.756	.776	.787
CSCNN [45]	.756	.775	.798
DeepContour [26]	.757	.776	.790
HFL [27]	.767	.788	.795
HED [7]	.788	.808	.840
RDS [46]	.792	.810	.818
DeepBounaries [8]	.813	.831	.866
CED-w/o-Multi	.794	.811	.847
CED	.803	.820	.871
CED-VOC-aug	.815	.833	.889
Improved-CED	.807	.824	.870
Improved-CED-VOC-aug	.817	.834	.887

TABLE II
COMPARISON TO THE STATE-OF-ARTS ON BSDS500 DATASET.

Recall curves of all methods for comparison. Without multi-scale testing, CED already achieves better results than the top-performing method [46] in all 3 metrics. Integrated with the multi-scale testing, CED achieves a further improvement, enhancing the ODS by 1.1%, OIS by 1.0% and AP by 5.3% in comparison to [46]. This result also surpasses the human benchmark on the BSDS500 dataset with ODS 0.8027. We note that the current record is from DeepBounaries [8], which used extra training samples ($> 10K$ images in VOC) and post-processing steps of global grouping. After simply augmenting the standard BSDS500 training dataset with VOC images as [8], without any post-processing steps, CED gives better results with ODS 0.815. The new form of CED is denoted as CED-VOC-aug.

We further benchmark the “crispness” of edges from CED. We report quantitative evaluation results by varying the matching distance d . The selected evaluation method should indicate whether the object contours can be precisely localized by tightened criteria. We evaluate CED on the following settings of d : d_0 , $d_0/2$, and $d_0/4$, where $d_0 = 4.3$ pixels. We compare the results with HED [7] and PMI [10], which also aims for generating crisp edges. The results are reported in the plot in Figure 8(a).

The performance of all methods decreases when d decreases. The gap between HED and PMI is getting closer with a smaller d . In contrast, the gap between CED and the two baselines stays fairly consistent. In fact, the ODS gap between CED and HED increases from 2.3% to 2.8%, the OIS gap increases from 2.3% to 2.9% and the AP gap increases from 4.2% to 9.1%. In addition, CED achieves ODS=0.606

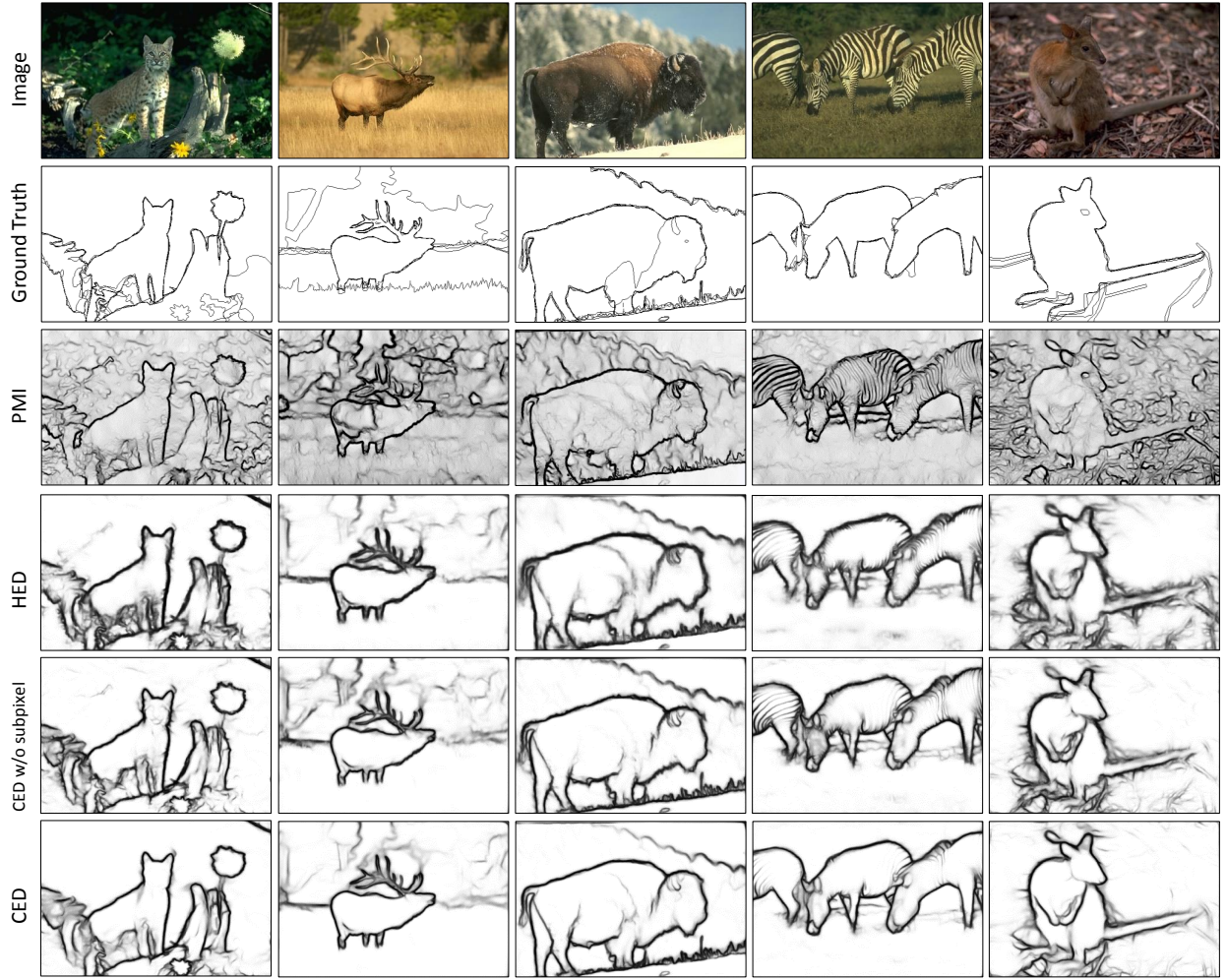


Fig. 7. Visualization of edge detection results from different methods. First two rows show the original images and ground-truths edges. The next four rows include the raw edge maps (before NMS) of PMI, HED, CED-w/o-Subpixel and CED, respectively. Edge maps from CED is sharper than HED and cleaner than PMI.

at the setting of $d_0/4$, approaching human level performance (0.625), and outperforming the methods in [10], [7] by a large margin. The results suggest that CED produces a crisp edge map.

Finally, Figure 7 shows a comparison of edge maps from PMI, HED and CED, before non-maximal suppression (NMS). Even without the standard non-maximal suppression (NMS), our method eliminates most blurry and noisy boundaries significantly. We observe that CED can produce cleaner, thinner and crisper image boundaries.

D. Improved CED

Maninis et al. [31] experiment with VGGNet and ResNet and show that the proposed network can leverage and benefit from improvements in the backbone network. Similarly, we also experiment with state-of-the-art network (ResNet-50 [15]) to replace original VGG-16 backbone network. What's more, as [16], we also improve the architecture of HED by adding another two convolutional layers at all five side-output layers. As discussed in [47], large kernel size helps to enable dense connections between feature maps and final classifiers, which

is conducive to cope with different transformations. The new added convolutional layers at side-output layers are equipped with larger filter size, especially for deeper layers, to further enlarge the receptive field. More specifically, the kernel size of new added convolutional layers for the five side-outputs is: 3x3, 3x3, 5x5, 5x5, 7x7. Similar modifications are adopted for original CED. The new term of HED and CED are denoted as Improved-HED and Improved-CED. As shown in Table III, Improved-HED and Improved-CED both achieve better results than original HED and CED. Compared with original CED, Improved-CED enhance the ODS from 0.803 to 0.807, achieving best recording results on standard BSDS500 dataset. As shown in Figure 6, after simply augmenting the standard BSDS500 training dataset with VOC images as [8], without complex post-processing steps, Improved-CED gives better results with ODS 0.817, outperforming all other state-of-the-art results. The new form of CED is denoted as Improved-CED-VOC-aug.

In addition, we also benchmark the "crispness" of boundaries generated with Improved-HED and Improved-CED. As shown in Figure 8(b), when the maximal permissible matching

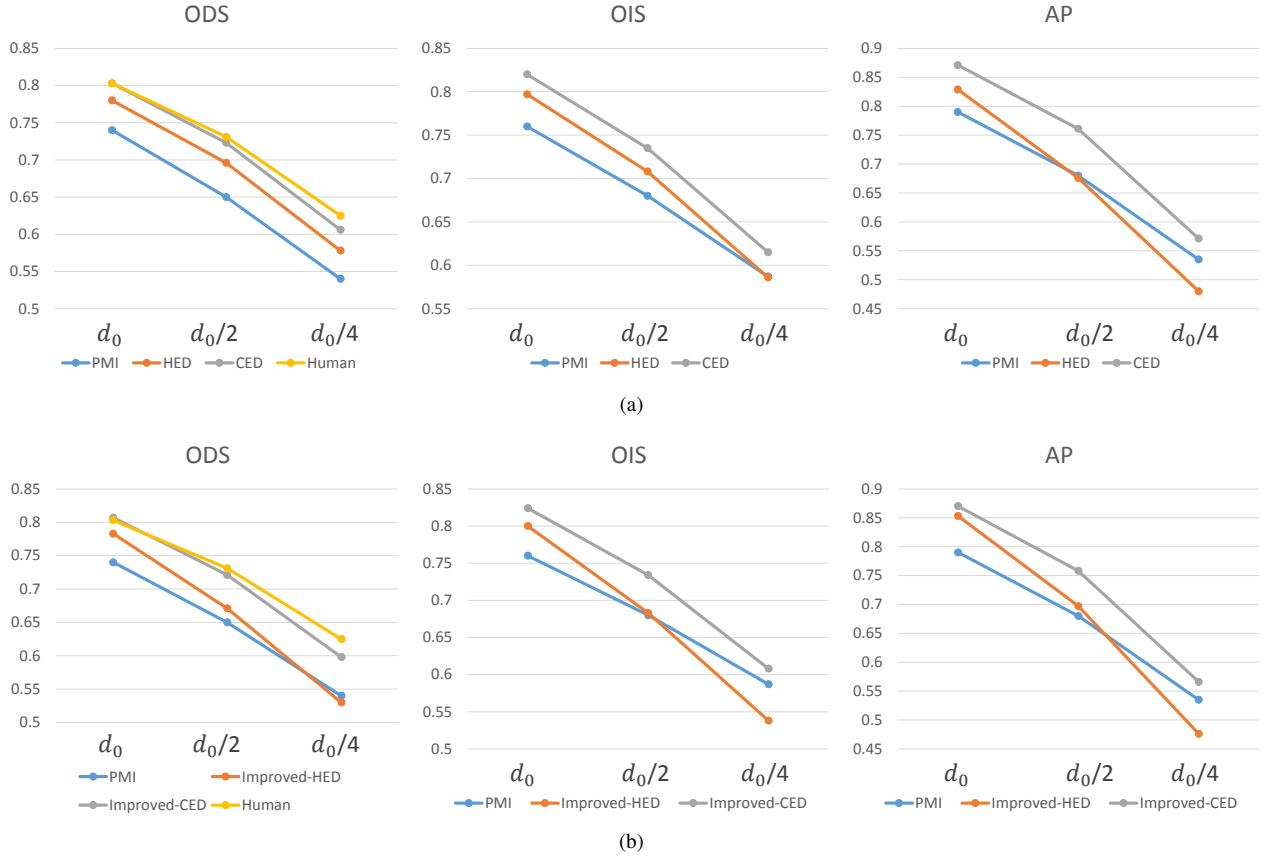


Fig. 8. We report the performance (ODS, OIS and AP) as a function of the maximal permissible distance d . (a) “Crispness” of boundaries generated with HED and CED; (b) “Crispness” of boundaries generated with Improved-HED and Improved-CED.

Method	ODS	OIS	AP
HED	.780	.797	.829
CED	.803	.820	.871
Improved-HED	.783	.800	.853
Improved-CED	.807	.824	.870

TABLE III

RESULTS ON BSDS500 WITH IMPROVED-HED AND IMPROVED-CED. IMPROVED-HED AND IMPROVED-CED BOTH ACHIEVE BETTER RESULTS THAN ORIGINAL HED AND CED RESPECTIVELY IN ALL THREE METRICS.

distance d decreases, the ODS gap between Improved-CED and Improved-HED increases from 2.5% to 6.8%, the OIS gap increases from 2.4% to 7.0% and the AP gap increases from 1.7% to 9.0%. These results suggest that Improved-CED produces a crisper edge map than Improved-HED. We can also find that Improved-CED achieves better results than CED at standard permissible matching distance d_0 , however, Improved-CED gets lower evaluation performance than original CED at $d_0/4$. Similar phenomenon can be observed between Improved-HED and original HED. This demonstrates the adversarial effect of deeper backbone network, it helps to achieve better boundary detection results at standard permissible matching distance, but weakens the localization ability.

VI. BENEFITS OF CRISP BOUNDARIES

As denoted in section I, boundary detection is critical for some higher-level vision tasks. We conduct experiments to

demonstrate the benefits of crisp boundaries for other related tasks. We plug in our method into optical flow estimation, object proposal generation and semantic segmentation, and evaluate its benefit for each task.

A. Datasets and Benchmarks

We benchmark optical flow estimation, object proposals generation and semantic segmentation method by applying our edge detector. The optical flow estimation results are reported on MPI Sintel dataset [48], a challenging optical flow evaluation benchmark obtained from animated sequences, and we use the final version with photo-realistic rendering. Similar to [3], [33], we report Average Endpoint Error (AEE) on the training set for optical flow estimation.

We benchmark object proposal generation results on Pascal VOC 2012 validation set (VOC12 val set) [49]. The VOC12 val set is composed of 1449 images from 20 common classes, such as “Train”, “Person” and “Sheep”. Since we use the edge detector trained only on BSDS500 dataset, we don’t need the Pascal VOC 2012 training set. The mean Jaccard index (mean best overlap) at instance level and class level are reported for the evaluation, as the same metrics in [4], [30]. More precisely, the Jaccard index at instance level (J_i) is the mean best overlap (intersection over union) for all the ground-truth instances in the dataset. The Jaccard index at class level (J_c) is the mean over the ground-truth instances within class c .

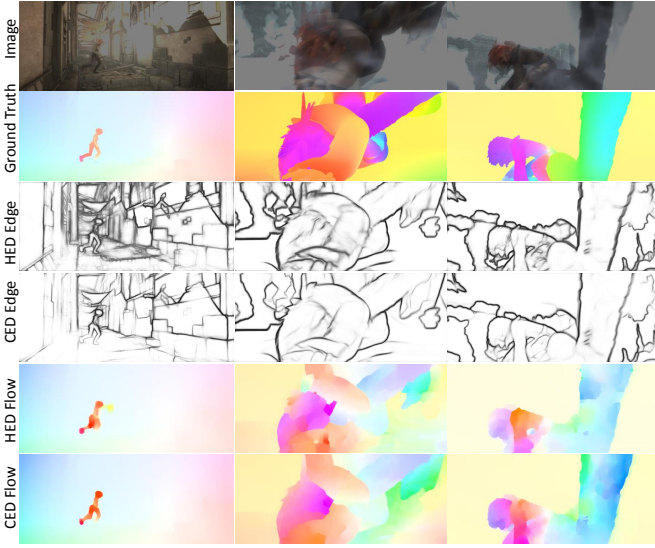


Fig. 9. Visualization of optical flow estimation results with different edge maps. From top to bottom: mean of two consecutive images, ground-truth flow, edge maps generated with HED and CED, and optical flow estimation results using these edge maps. CED produces better motion details, such as the leg of the girl in the first image.

The benefits of crisp boundaries for semantic segmentation are evaluated on Pascal Context dataset [50], which provides the whole scene labeling for 10103 images including both object and stuff. The whole dataset is split into training set and validation set, which contains 4998 and 5105 images respectively. We evaluate on the most frequent 59 classes along with the background category, as [51]. Pixel accuracy (PA), mean pixel accuracy (MPA), mean intersection over union (Mean IOU) are adopted as evaluation metrics. More concretely, PA computes a ratio between the amount of properly classified pixels and the total number of them, MPA stands for the average value of ratio of correct pixels per-class, while Mean IOU means the ratio between the intersection and the union of the ground truth and predicted segmentation.

B. Optical Flow with Crisp Boundaries

To analyze the benefits of crisp edges, we plug in HED and CED results for optical flow estimation, an mid-level vision task. Optical flow estimation, an important and challenging problem, aims to capture the motion information between neighboring frames in image sequence. We choose EpicFlow [3] as our optical flow estimation method. EpicFlow computes geodesic distance using an edge map, which is further used to interpolate sparse matches from [52]. Thus, an accurate edge map is important for good optical flow estimation results. We compare CED results with HED. In this case, we train CED and HED on BSDS500 and test it on Sintel. The AEE on Sintel training set using CED is 3.570 while HED gives 3.588. This result illustrates that the optical flow can benefit from a better localized edge map. Figure 9 shows the visualization of sample flow maps from Sintel. Again, CED get slightly more accurate flow results than HED.

C. Object Proposals with Crisp Boundaries

We also demonstrate the benefit of the crisp edge map for object proposals generation. Object proposals generation, another important mid-level vision task, is the first step for other higher-level tasks, such as object detection. We choose the Multi-scale Combinatorial Grouping (MCG) and its single scale version (SCG) in [4] to generate object proposals. With an input edge map, MCG builds a hierarchical grouping of contours to generate object proposals. The original MCG adopts the Structured Edge (SE) [53] as the default edge detector. We simply replace the edge detector with HED [7] and CED. Note that HED and CED are both trained only on the BSDS500 dataset. We benchmark the combination of three edge detectors (SE, HED, CED) with both MCG and SCG.

We report the mean Jaccard index at both instance level and class level with respect to the number of proposals in Figure 10. CED-MCG achieves the best results at both metrics for all number of proposals. Table IV further compares the Jaccard index at instance level for each class at two operation points of N_c , namely the top-100 proposals and all proposals. Our method outperforms HED by 4.6% with top-100 proposals, and by 2.7% with all proposals. These results further demonstrate the benefits of crisp edges.

D. Semantic Segmentation with Crisp Boundaries

We also demonstrate the benefit of crisp boundaries for semantic segmentation. Semantic segmentation, an important high-level vision task, aims at dense pixel-level classification from predefined set of categories. Semantic segmentation has witnessed rapid development with the help of fully convolutional networks (FCNs) [17]. However, as discussed in [18], due to the large receptive field of convolutional layers and largely reduced resolution of successive down-sampling layers, segments generated by FCN-based methods are blob-like and are poorly localized around object boundaries. Some post-processing procedure are introduced to alleviate this issue. Instead of using color affinity functions as [51], [18] proposed Boundary Neural Field (BNF) which is characterized with boundary-based pixel affinity functions and a global optimization strategy. BNF computes affinity between two pixels with an input edge map, the larger the magnitude value of the boundary crossing the straight path between the two pixels, the lower affinity between the two pixels. Thus crisper boundaries encourage more accurate pixel affinities estimation. The original BNF adopts edge map generated with a linear combination of interpolated convolutional feature maps inside the FCN. We simply replace it with HED and CED results. Similarly, HED and CED are both trained only on BSDS500 dataset. We choose Deeplab [51] to generate initial segmentation result and BNF with different edge detectors as the final post-processing step.

We report pixel accuracy (PA), mean pixel accuracy (MPA) and mean intersection over union (Mean IOU) on Pascal Context test set as shown in Table V. And HED and CED are both retrained on the Pascal Context train set. The initial Deeplab achieves a Mean IOU of 42.6%, the evaluation results after post-processing procedure of BNF with edge map

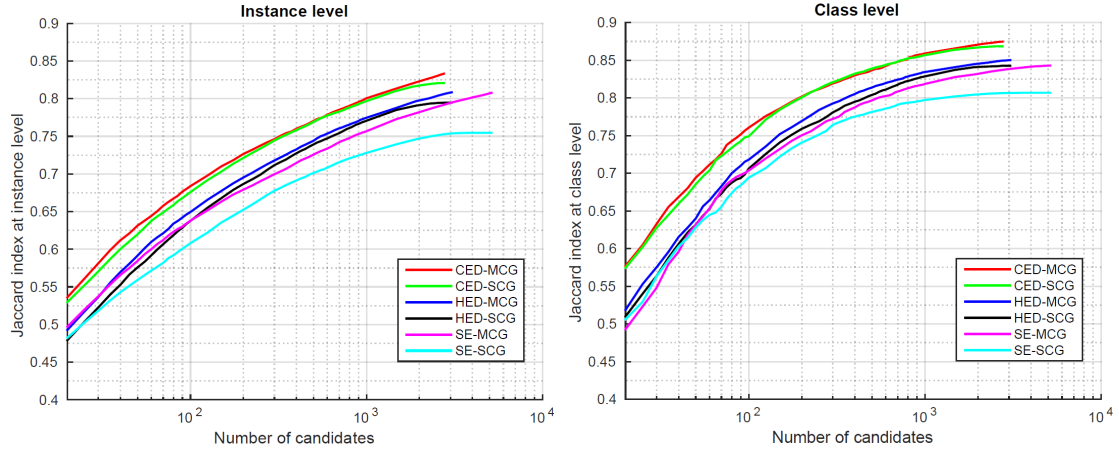


Fig. 10. Object proposals performance on VOC12 val set at instance level (left) and class level (right). We evaluate three different edge detectors (SE, HED, CED) with two grouping methods (MCG, SCG), and report curve of the mean Jaccard index with respect to all number of proposals. CED-MCG achieves the best results.

	Nc	Plane	Bicycle	Bird	Boat	Bottle	Bus	Car	Cat	Chair	Cow	Table	Dog	Horse	MBike	Person	Plant	Sheep	Sofa	Train	TV	Global
SE-MCG	100	71.2	38.6	74.7	64.5	53.7	70.6	48.9	82.7	55.4	79.1	66.7	78.8	70.6	65.4	60.4	49.9	71.9	73.7	71.3	76.2	63.8
HED-MCG	100	73.0	39.3	79.9	70.0	56.2	68.8	50.7	86.9	55.1	81.6	62.7	85.0	73.7	63.9	59.2	56.5	76.2	72.6	68.6	73.6	64.9
CED-MCG	100	78.2	42.2	85.1	72.3	55.2	76.4	56.0	90.5	56.2	83.6	68.2	88.2	76.9	70.2	62.8	55.7	78.8	77.4	78.2	75.3	68.4
SE-MCG	5138	83.0	51.2	86.4	79.7	78.1	81.8	77.4	90.8	74.5	88.7	84.2	88.1	81.4	78.6	79.7	77.5	86.7	87.8	81.9	90.3	80.8
HED-MCG	3051	83.3	52.2	87.8	81.5	77.3	80.4	78.3	94.2	74.2	90.8	82.6	92.2	84.0	76.9	78.4	75.5	90.0	87.6	80.0	87.9	80.8
CED-MCG	2757	86.8	54.7	90.3	82.7	77.5	86.9	82.2	95.1	77.1	2.0	84.6	93.2	86.2	80.8	80.8	78.8	91.0	89.4	86.3	89.6	83.3

TABLE IV

OBJECT PROPOSALS PERFORMANCE ON VOC12 VAL SET WITH TOP-100 AND ALL PROPOSALS. WE REPORT PER-CLASS AND MEAN JACCARD INDEX (MEAN BEST OVERLAP) AT INSTANCE LEVEL. OUR CED CLEARLY OUTPERFORMS ALL OTHER EDGE DETECTORS.

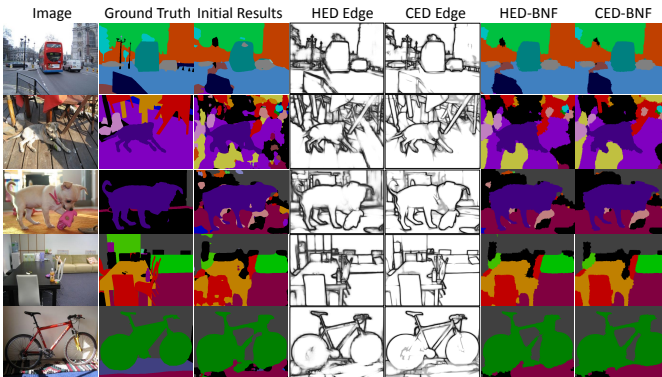


Fig. 11. Sample semantic segmentation results on Pascal Context val set. With two different edge detectors (HED, CED), we post-process the initial results produced by Deeplab with BNF. With sharp and clean edge maps (CED edge), CED-BNF achieves better segmentation results, and captures more precise details along object contour.

generated by HED and CED are both improved. And CED-BNF get best results on all three evaluation metrics. Figure 11 shows the initial semantic segmentation results of Deeplab, edge maps with HED and CED, post-processed semantic segmentation results with HED-BNF and CED-BNF. With clean and sharp boundaries (CED edge), CED-BNF improve the initial segmentation results with more details along the object contour. These results demonstrate the benefit of crisp boundaries for semantic segmentation.

	PA	MPA	Mean IOU
Deeplab	70.7	54.5	42.6
HED-BNF	72.1	55.4	44.1
CED-BNF	72.3	55.5	44.3

TABLE V

SEMANTIC SEGMENTATION RESULTS ON PASCAL CONTEXT VAL SET. WITH TWO DIFFERENT EDGE DETECTORS (HED, CED), WE POST-PROCESS THE INITIAL RESULTS PRODUCED BY DEEPLAB WITH BNF. WITH MORE PRECISE DETAILS ALONG THE OBJECT CONTOUR, CED-BNF ACHIEVES BEST RESULTS.

VII. CED FOR SALIENCY DETECTION

In this section, we demonstrate that same architecture as CED can achieve state-of-the-art results on saliency detection task. Visual saliency detection, an important and fundamental task, aims to detect the most distinct objects or regions in an image. Many computer vision tasks require saliency detection results for later processing, such as image retrieval [54] and image segmentation [55]. Traditional saliency detection methods depend on low-level features [56] or high-level information [57]. Instead of using these hand-crafted features, ConvNet-based methods have outperformed traditional methods by a large margin in patch-based [58] or pixel-level way [19].

Similar to boundary detection, saliency detection can be processed as a pixel-level saliency estimation task. Both two tasks generate dense pixel-level response map, with each pixel indicating the probability of the corresponding pixel belonging to salient region or object boundary. So the HED and our CED network can be easily generalized to visual saliency detection task, even without network architecture modifications.

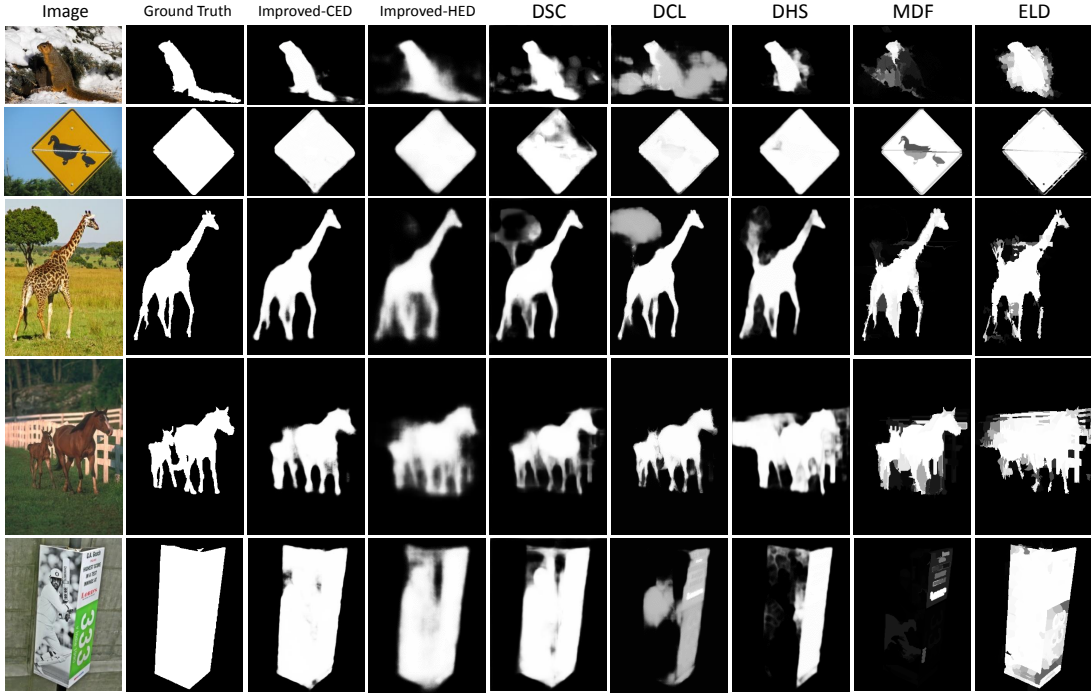


Fig. 12. Visual comparison with different saliency detection methods. Compared to Improved-HED (the fourth column), Improved-CED (the third column) produces more precise saliency map and exhibits higher contrast between salient region and background clearly. In addition, Improved-CED produces more complete saliency details especially along the object boundaries than other state-of-arts.

A. Datasets and Evaluation Metrics

Following [16], we evaluate HED and CED on 5 widely used benchmark datasets: MSRA-B [56], ECSSD [59], HKU-IS [58], PASCAL-S [60], and SOD [61], [62]. MSRA-B contains 5000 images with mostly one salient object. The dataset is divided into train set, validation set, and test set, containing 2,500, 500, 2,000 images respectively. This dataset are collected from hundreds of common categories, such as "person", "horse" and "flower". ECSSD is composed of 1,000 challenging images with complex background. HKU-IS is a new large and challenging dataset created with 4447 natural images. Dissimilar with MSRA-B dataset which typically include a single salient object located in center of images, image in HKU-IS dataset is more likely to contain multiple salient objects with diverse locations. PASCAL-S dataset is built on the validation set of the PASCAL VOC [49] 2010 segmentation challenge, containing 850 challenging images with cluttered backgrounds. SOD, built upon Berkeley Segmentation Dataset (BSD)[2], [9], consists of 300 images with multiple complex salient objects. For consistency with existing methods [16], [63], we train HED and CED only on MSRA-B train set and validation set, which is composed of 3000 images, and evaluate the trained models on MSRA-B test set, and all other four datasets.

Two standard evaluation metrics, F-measure (F_β) and the mean absolute error (MAE), are used to evaluate HED and CED. For a given continuous saliency map, we can convert it to a binary mask using a threshold. The F-measure represents the comprehensive performance of the saliency detection results, which takes into account the precision and

recall. Precision refers to the percentage of salient pixels correctly predicted, and recall corresponds to the proportion of predicted salient pixels to the ground-truth salient pixels. As discussed in [64], F-measure is an overlap-based evaluation measures, which neglect the pixels correctly marked as non-salient. In addition, the weighted, continuous saliency maps is more important than binary masks (adopted for F-measure) in some applications[65]. A more comprehensive evaluation metrics should be adopted. The MAE computes the average per-pixel difference between the ground-truth annotation and the predicted salient map.

B. Ablation Study

To conduct ablation analysis, we first benchmark HED and CED on PASCAL-S. And note that no post-processing steps, such as conditional random field (CRF[67]) based smoothing methods, are adopted in our experiments. As Table VII shows, HED achieves a F-measure of 0.801, while CED boosts the performance by 0.7%. This demonstrates the effectiveness of CED for saliency detection. Then we experiment with Improved-HED and Improved-CED mentioned in V-D. Besides ResNet50 based Improved-HED and Improved-CED, we also replace the backbone network with VGG16, termed with VGG16-Improved-HED and VGG16-Improved-CED respectively. VGG16-Improved-HED achieves a F-measure of 0.822, higher than vanilla HED by a large margin (2.1%). VGG16-Improved-CED further improves over VGG16-Improved-HED by another 0.9%, outperforming most state-of-arts even without any post-processing steps. When replaced with ResNet50 as the backbone network, Improved-

Datasets	MSRA-B		ECSSD		HKUI-IS		PASCALS		SOD	
Evaluation Criteria	F_β	MAE	F_β	MAE	F_β	MAE	F_β	MAE	F_β	MAE
GC	0.817	0.138	0.741	0.187	0.726	0.165	0.640	0.225	0.657	0.242
DRFI	0.855	0.119	0.787	0.166	0.783	0.143	0.679	0.221	0.712	0.215
MC	0.872	0.062	0.822	0.107	0.781	0.098	0.721	0.147	0.708	0.184
ELD	0.914	0.042	0.865	0.981	0.844	0.071	0.767	0.121	0.760	0.154
MDF	0.885	0.104	0.833	0.108	0.860	0.129	0.764	0.145	0.785	0.155
DHS	-	-	0.905	0.061	0.892	0.052	0.820	0.091	0.823	0.127
DCL	0.916	0.047	0.898	0.071	0.907	0.048	0.822	0.108	0.832	0.126
DSC	0.926	0.029	0.915	0.055	0.912	0.040	0.831	0.083	0.842	0.121
Improved-HED	0.914	0.054	0.904	0.072	0.886	0.064	0.826	0.113	0.822	0.114
Improved-CED	0.929	0.035	0.922	0.051	0.910	0.041	0.846	0.100	0.842	0.099
Improved-CED-CRF	0.933	0.032	0.931	0.046	0.920	0.035	0.852	0.097	0.852	0.095

TABLE VI

COMPARISONS WITH STATE-OF-ARTS ON FIVE WIDELY USED DATASETS. THE TOP THREE RESULTS ARE HIGHLIGHTED IN RED, GREEN, AND BLUE, RESPECTIVELY. EVEN WITHOUT SOPHISTICATED CRF BASED POST-PROCESSING STEPS, IMPROVED-CED ACHIEVES STATE-OF-THE-ART RESULTS. AFTER PROCESSED WITH CRF BASED POST-PROCESSING AS [16], [66], IMPROVED-CED-CRF ACHIEVES BETTER RESULTS.

Architecture	F_β
HED	0.801
CED	0.808
VGG16-Improved-HED	0.822
VGG16-Improved-CED	0.831
Improved-HED	0.826
Improved-CED	0.846

TABLE VII

THE PERFORMANCE OF DIFFERENT NETWORK ARCHITECTURE SETTINGS ON PASCAL-S DATASET. VANILLA CED ACHIEVES BETTER RESULT THAN HED BY 0.7%, VGG16-IMPROVED-CED IMPROVES OVER CED BY 2.3% AND OBTAINS BETTER PERFORMANCE THAN VGG16-IMPROVED-HED AGAIN. WITH RESNET50 AS BACKBONE NETWORK, IMPROVED-CED BOOSTS THE PERFORMANCE BY ANOTHER 1.5% COMPARED TO VGG16-IMPROVED-CED, AND ACHIEVES MUCH BETTER RESULT THAN IMPROVED-HED.

HED and Improved-CED both get better performance, with F-measure of 0.826 and 0.846 respectively. And note that since we observe no gain with multi-scale evaluation strategy, we evaluate with single-scale image in testing phase. What's more, as shown in Figure 12, compared to Improved-HED (the fourth column), Improved-CED (the third column) produces much more precise saliency map and exhibits higher contrast between salient region and background clearly. Both quantitative and qualitative results suggest the superior performance of CED network to HED.

C. Comparison with state-of-arts

We compare the best performing Improved-CED with 6 existing ConvNet-based methods, including MDF[58], DCL[66], ELD[68], MC[69], DHS[19], and DSC[16], and another 2 classic methods, GC[70], and DRFI[63]. We compare our approach with previous methods in terms of F-measure and MAE score. The detailed results are listed in Table VI. Without complex CRF based post-processing steps, Improved-CED already achieves state-of-the-art results. After processed with CRF based post-processing as [16], [66],

Improved-CED-CRF obtains better results. Figure 12 provides a visual comparison of our approach with respect to previous methods. Improved-CED captures more complete saliency details especially along the object boundaries.

VIII. CONCLUSION

We showed that ConvNet based edge detector tends to generate edge maps which are not well aligned with image boundaries. We discussed the reason behind the issue and proposed a novel architecture that largely improved its localization ability. Our detector achieved promising performance on BSDS500, outperforming the state-of-the-art methods when using strict maximum tolerance setting. We verified the benefits of crisp edge map for optical flow estimation, object proposals generation and semantic segmentation, covering mid-level and high-level vision tasks. Finally, we showed that our proposed network can be easily generalized to salient region detection task, and the proposed network achieves state-of-the-art performance on five widely used saliency detection benchmark. And we believe that our proposed network can also be extended to diverse dense pixel labeling tasks, such as semantic segmentation, depth prediction.

Our work looked into edge detection, a classical problem in computer vision. We hope that it will provide a reflection of the recent victory of ConvNet in computer vision. While we are getting better results from standard quantitative evaluations, the fundamental vision problem still remains open. It is probably the right time to revisit our evaluation criteria.

REFERENCES

- [1] W. Yupei, Z. Xin, and K. Huang, "Deep crisp boundaries," in *CVPR*, 2017.
- [2] D. R. Martin, C. C. Fowlkes, and J. Malik, "Learning to detect natural image boundaries using local brightness, color, and texture cues," *TPAMI*, 2004.
- [3] J. Revaud, P. Weinzaepfel, Z. Harchaoui, and C. Schmid, "Epicflow: Edge-preserving interpolation of correspondences for optical flow," in *CVPR*, 2015.
- [4] P. Arbeláez, J. Pont-Tuset, J. T. Barron, F. Marques, and J. Malik, "Multiscale combinatorial grouping," in *CVPR*, 2014.

- [5] N. Dalal and B. Triggs, "Histograms of oriented gradients for human detection," in *CVPR*, vol. 1. IEEE, 2005.
- [6] P. Dollar, Z. Tu, and S. Belongie, "Supervised learning of edges and object boundaries," in *CVPR*. IEEE, 2006.
- [7] S. Xie and Z. Tu, "Holistically-nested edge detection," in *ICCV*, 2015.
- [8] I. Kokkinos, "Pushing the boundaries of boundary detection using deep learning," *ICLR*, 2016.
- [9] P. Arbelaez, M. Maire, C. Fowlkes, and J. Malik, "Contour detection and hierarchical image segmentation," *TPAMI*, 2011.
- [10] P. Isola, D. Zoran, D. Krishnan, and E. H. Adelson, "Crisp boundary detection using pointwise mutual information," in *ECCV*, 2014.
- [11] A. Krizhevsky, I. Sutskever, and G. E. Hinton, "Imagenet classification with deep convolutional neural networks," in *NIPS*, 2012.
- [12] X. Ren, "Local grouping for optical flow," in *CVPR*, 2008.
- [13] P. O. Pinheiro, T.-Y. Lin, R. Collobert, and P. Dollár, "Learning to refine object segments," in *ECCV*, 2016.
- [14] W. Shi, J. Caballero, F. Huszár, J. Totz, A. P. Aitken, R. Bishop, D. Rueckert, and Z. Wang, "Real-time single image and video super-resolution using an efficient sub-pixel convolutional neural network," in *CVPR*, 2016.
- [15] K. He, X. Zhang, S. Ren, and J. Sun, "Deep residual learning for image recognition," in *CVPR*, 2016.
- [16] Q. Hou, M.-M. Cheng, X.-W. Hu, A. Borji, Z. Tu, and P. Torr, "Deeply supervised salient object detection with short connections," *arXiv preprint arXiv:1611.04849*, 2016.
- [17] E. Shelhamer, J. Long, and T. Darrell, "Fully convolutional networks for semantic segmentation," *TPAMI*, 2017.
- [18] G. Bertasius, J. Shi, and L. Torresani, "Semantic segmentation with boundary neural fields," in *CVPR*, 2016.
- [19] N. Liu and J. Han, "Dhsnet: Deep hierarchical saliency network for salient object detection," in *CVPR*, 2016.
- [20] J. R. Fram and E. S. Deutsch, "On the quantitative evaluation of edge detection schemes and their comparison with human performance," *IEEE Transactions on Computers*.
- [21] J. Canny, "A computational approach to edge detection," *TPAMI*.
- [22] W. T. Freeman, E. H. Adelson *et al.*, "The design and use of steerable filters," *TPAMI*, 1991.
- [23] J. J. Lim, C. L. Zitnick, and P. Dollár, "Sketch tokens: A learned mid-level representation for contour and object detection," in *CVPR*, 2013.
- [24] R. Xiao-feng and L. Bo, "Discriminatively trained sparse code gradients for contour detection," in *NIPS*, 2012.
- [25] G. Bertasius, J. Shi, and L. Torresani, "Deepedge: A multi-scale bifurcated deep network for top-down contour detection," in *CVPR*, 2015.
- [26] W. Shen, X. Wang, Y. Wang, X. Bai, and Z. Zhang, "Deepcontour: A deep convolutional feature learned by positive-sharing loss for contour detection," in *CVPR*, 2015.
- [27] G. Bertasius, J. Shi, and L. Torresani, "High-for-low and low-for-high: Efficient boundary detection from deep object features and its applications to high-level vision," in *ICCV*, 2015.
- [28] E. Shelhamer, J. Long, and T. Darrell, "Fully convolutional networks for semantic segmentation," *TPAMI*, 2017.
- [29] C.-Y. Lee, S. Xie, P. Gallagher, Z. Zhang, and Z. Tu, "Deeply-supervised nets," in *AISTATS*, vol. 2, no. 3, 2015, p. 6.
- [30] J. Yang, B. Price, S. Cohen, H. Lee, and M.-H. Yang, "Object contour detection with a fully convolutional encoder-decoder network," in *CVPR*, 2016.
- [31] K. Maninis, J. Pont-Tuset, P. Arbeláez, and L. V. Gool, "Convolutional oriented boundaries: From image segmentation to high-level tasks," *TPAMI*, 2017.
- [32] A. Khoreva, R. Benenson, M. Omran, M. Hein, and B. Schiele, "Weakly supervised object boundaries," in *CVPR*, 2016.
- [33] Y. Li, M. Paluri, J. M. Rehg, and P. Dollár, "Unsupervised learning of edges," in *CVPR*, 2016.
- [34] K. He, G. Gkioxari, P. Dollár, and R. Girshick, "Mask r-cnn," *arXiv preprint arXiv:1703.06870*, 2017.
- [35] A. Bansal, X. Chen, B. Russell, A. G. Ramanan *et al.*, "Pixelnet: Representation of the pixels, by the pixels, and for the pixels," *arXiv preprint arXiv:1702.06506*, 2017.
- [36] W. Shi, J. Caballero, F. Huszár, J. Totz, A. P. Aitken, R. Bishop, D. Rueckert, and Z. Wang, "Real-time single image and video super-resolution using an efficient sub-pixel convolutional neural network," in *CVPR*, 2016.
- [37] M. D. Zeiler, G. W. Taylor, and R. Fergus, "Adaptive deconvolutional networks for mid and high level feature learning," in *ICCV*, 2011.
- [38] V. Dumoulin and F. Visin, "A guide to convolution arithmetic for deep learning," *arXiv preprint arXiv:1603.07285*, 2016.
- [39] A. Vedaldi and K. Lenc, "Matconvnet: Convolutional neural networks for matlab," in *ACMMM*, 2015.
- [40] Y. Jia, E. Shelhamer, J. Donahue, S. Karayev, J. Long, R. Girshick, S. Guadarrama, and T. Darrell, "Caffe: Convolutional architecture for fast feature embedding," *arXiv preprint arXiv:1408.5093*, 2014.
- [41] P. Dollár and C. L. Zitnick, "Fast edge detection using structured forests," *TPAMI*, 2015.
- [42] A. Sironi, V. Lepetit, and P. Fua, "Projection onto the manifold of elongated structures for accurate extraction," in *ICCV*, 2015.
- [43] J. J. Kivinen, C. K. Williams, N. Heess, and D. Technologies, "Visual boundary prediction: A deep neural prediction network and quality dissection," in *AISTATS*, 2014.
- [44] A. Sironi, E. Türetken, V. Lepetit, and P. Fua, "Multiscale centerline detection," *TPAMI*, 2016.
- [45] J.-J. Hwang and T.-L. Liu, "Pixel-wise deep learning for contour detection," *arXiv preprint arXiv:1504.01989*, 2015.
- [46] Y. Liu and M. S. Lew, "Learning relaxed deep supervision for better edge detection," in *CVPR*, 2016.
- [47] C. Peng, X. Zhang, G. Yu, G. Luo, and J. Sun, "Large kernel matters—improve semantic segmentation by global convolutional network," *arXiv preprint arXiv:1703.02719*, 2017.
- [48] D. J. Butler, J. Wulff, G. B. Stanley, and M. J. Black, "A naturalistic open source movie for optical flow evaluation," in *ECCV*, 2012.
- [49] M. Everingham, L. Van Gool, C. K. Williams, J. Winn, and A. Zisserman, "The pascal visual object classes (voc) challenge," *IJCV*, 2010.
- [50] R. Mottaghi, X. Chen, X. Liu, N.-G. Cho, S.-W. Lee, S. Fidler, R. Urtasun, and A. Yuille, "The role of context for object detection and semantic segmentation in the wild," in *CVPR*, 2014.
- [51] L.-C. Chen, G. Papandreou, I. Kokkinos, K. Murphy, and A. L. Yuille, "Deeplab: Semantic image segmentation with deep convolutional nets, atrous convolution, and fully connected crfs," *arXiv preprint arXiv:1606.00915*, 2016.
- [52] P. Weinzaepfel, J. Revaud, Z. Harchaoui, and C. Schmid, "Deepflow: Large displacement optical flow with deep matching," in *CVPR*, 2013.
- [53] P. Dollár and C. L. Zitnick, "Structured forests for fast edge detection," in *ICCV*, 2013.
- [54] Y. Gao, M. Wang, Z.-J. Zha, J. Shen, X. Li, and X. Wu, "Visual-textual joint relevance learning for tag-based social image search," *TIP*, 2013.
- [55] C. Jung and C. Kim, "A unified spectral-domain approach for saliency detection and its application to automatic object segmentation," *TIP*, 2012.
- [56] T. Liu, Z. Yuan, J. Sun, J. Wang, N. Zheng, X. Tang, and H.-Y. Shum, "Learning to detect a salient object," *TPAMI*, 2011.
- [57] S. Goferman, L. Zelnik-Manor, and A. Tal, "Context-aware saliency detection," *TPAMI*, 2012.
- [58] G. Li and Y. Yu, "Visual saliency based on multiscale deep features," in *CVPR*, 2015.
- [59] Q. Yan, L. Xu, J. Shi, and J. Jia, "Hierarchical saliency detection," in *CVPR*, 2013.
- [60] Y. Li, X. Hou, C. Koch, J. M. Rehg, and A. L. Yuille, "The secrets of salient object segmentation," in *CVPR*, 2014.
- [61] D. Martin, C. Fowlkes, D. Tal, and J. Malik, "A database of human segmented natural images and its application to evaluating segmentation algorithms and measuring ecological statistics," in *ICCV*, 2001.
- [62] V. Movahedi and J. H. Elder, "Design and perceptual validation of performance measures for salient object segmentation," in *CVPRW*. IEEE, 2010.
- [63] H. Jiang, J. Wang, Z. Yuan, Y. Wu, N. Zheng, and S. Li, "Salient object detection: A discriminative regional feature integration approach," in *CVPR*, 2013.
- [64] A. Borji, M.-M. Cheng, H. Jiang, and J. Li, "Salient object detection: A benchmark," *TIP*, vol. 24, no. 12, pp. 5706–5722, 2015.
- [65] S. Avidan and A. Shamir, "Seam carving for content-aware image resizing," in *ACM Transactions on graphics*. ACM, 2007.
- [66] G. Li and Y. Yu, "Deep contrast learning for salient object detection," in *CVPR*, 2016.
- [67] P. Krähenbühl and V. Koltun, "Efficient inference in fully connected crfs with gaussian edge potentials," in *NIPS*, 2011.
- [68] G. Lee, Y.-W. Tai, and J. Kim, "Deep saliency with encoded low level distance map and high level features," in *CVPR*, 2016.
- [69] R. Zhao, W. Ouyang, H. Li, and X. Wang, "Saliency detection by multi-context deep learning," in *CVPR*, 2015.
- [70] M.-M. Cheng, N. J. Mitra, X. Huang, P. H. Torr, and S.-M. Hu, "Global contrast based salient region detection," *TPAMI*, 2015.